University of Reading

Physical factors influencing regional precipitation variability attributed using an airmass trajectory method

Article

Published Version

De Leeuw, J., Methven, J. ORCID: https://orcid.org/0000-0002-7636-6872 and Blackburn, M. (2017) Physical factors influencing regional precipitation variability attributed using an airmass trajectory method. Journal of Climate, 30 (18). pp. 7359-7378. ISSN 1520-0442 doi: 10.1175/JCLI-D-16-0547.1 Available at https://centaur.reading.ac.uk/67132/

It is advisable to refer to the publisher's version if you intend to cite from the work. See Guidance on citing.
Published version at: http://doi.org/10.1175/JCLI-D-16-0547.1
To link to this article DOI: http://dx.doi.org/10.1175/JCLI-D-16-0547.1

Publisher: American Meteorological Society

All outputs in CentAUR are protected by Intellectual Property Rights law, including copyright law. Copyright and IPR is retained by the creators or other copyright holders. Terms and conditions for use of this material are defined in the End User Agreement.

www.reading.ac.uk/centaur

University of Reading

CentAUR

Central Archive at the University of Reading

Reading's research outputs online

Physical Factors Influencing Regional Precipitation Variability Attributed Using an Airmass Trajectory Method

JOHANNES DE LEEUW AND JOHN METHVEN

Department of Meteorology, University of Reading, Reading, United Kingdom

MICHAEL BLACKBURN

National Centre for Atmospheric Science, University of Reading, Reading, United Kingdom

(Manuscript received 20 August 2016, in final form 31 March 2017)

ABSTRACT

A novel Lagrangian framework is developed to attribute monthly precipitation variability to physical processes. Precipitation variability is partitioned into a combination of five factors: airmass origin location, origin surface temperature variation, ascent intensity, mass fraction of ascending air, and the number of ''wet'' analysis times per month [>1 mm $(6\,\mathrm{h})^{-1}$]. Precipitation in a target region is linked to ''origin'' locations of air masses where the water vapor mixing ratio was last set by boundary layer moistening and is a maximum along back trajectories. Applying the technique to the England and Wales region, the factors together account for 83%–89% of the observed summer precipitation variability. The dominant contributor is the number of wet analyses, which is shown to be associated with cyclone statistics. The wettest summer months are mainly associated with anomalous cyclone duration rather than the number of cyclones. In addition, surface temperature and saturation humidity at the origin locations are found to be below their climatological averages (1979–2013). Therefore, the direct thermodynamic effect of anomalous surface temperature on marine boundary layer humidity acts to reduce monthly precipitation anomalies. The decadal precipitation change between phases of the Atlantic multidecadal oscillation is approximately 20% of the interannual variability between summer months. Changes in cyclone statistics have an effect 6 times larger than the direct thermodynamic factor in both monthly and decadal precipitation variability.

1. Introduction

Regional precipitation accumulations across the Northern Hemisphere have been observed and studied using a wide range of observation types, varying from surface rain gauges (Wigley et al. 1984; Trenberth et al. 2007) to estimates retrieved using calibrated satellite data (Prihodko and Goward 1997; Ebert et al. 2007) or a blend of these (Huffman et al. 2009). However, determining whether regional precipitation climates have significantly changed in the past century remains difficult (Alexander et al. 2006), partly because of the large interannual variability.

Projected precipitation changes in future climate scenarios are also uncertain (Allen and Ingram 2002; Trenberth et al. 2003; Held and Soden 2006; Allan and Soden 2008). The IPCC Fifth Assessment Report states in chapter 11: ''Zonal mean precipitation will *very likely* increase in high and some of the mid latitudes, and will *more likely than not* decrease in the subtropics. At more regional scales precipitation changes may be influenced by anthropogenic aerosol emissions and will be strongly influenced by natural internal variability'' (Kirtman et al. 2013, p. 956).

A thermodynamic argument often put forward is that higher surface temperatures imply higher saturation vapor pressure (via the Clausius–Clapeyron relation), greater moisture loading within air masses, and hence greater precipitation within storms, all other things being equal (Pall et al. 2007; Trenberth 2011). However, one major uncertainty missing in this simple thermodynamic argument is the role of changing atmospheric circulation (Shepherd 2014). The IPCC report states that there is only ''medium'' confidence in near-term projections of the Northern Hemisphere extratropical circulation (Kirtman et al. 2013). It has been established that global average precipitation is strongly constrained by the global energy budget (Allen and Ingram 2002),

Corresponding author: J. de Leeuw, j.deleeuw1@uu.nl

DOI: 10.1175/JCLI-D-16-0547.1

© 2017 American Meteorological Society. For information regarding reuse of this content and general copyright information, consult the AMS Copyright Policy (www.ametsoc.org/PUBSReuseLicenses).

although it has been argued that the thermodynamic argument (Clausius–Clapeyron relation) still applies to global precipitation extremes (Allan and Soden 2008). However, vertical motion is required for precipitation, and a more complete argument must consider the dynamics of weather systems. In the midlatitude storm tracks, cyclones dominate the vertical motion. Hawcroft et al. (2012) used reanalysis and cyclone-track calculations to estimate that more than 70% of precipitation in northwest Europe is associated with the passage of extratropical cyclones from the North Atlantic storm track. Hence, in regions such as western Europe, changes in the storm track will have a major influence on precipitation variability. Despite a number of studies investigating precipitation trends and variability over Europe (Pauling et al. 2006; Frei et al. 2006; Nikulin et al. 2011; Rajczak et al. 2013), much is still unknown about the physical mechanisms responsible for the observed temporal variability. Most studies have not attempted a quantitative attribution of precipitation accumulations and their variability to the physical mechanisms responsible.

Lagrangian models have proven to be a useful tool in analyzing precipitation variability and precipitation extremes (James et al. 2004; Stohl and James 2004; Sodemann and Zubler 2010; Winschall et al. 2014), as these enable the investigation of water vapor transport within air masses along their path toward a region of interest. Trajectories make a link between the important moisture sources, conditions at those locations, and their influence on precipitable water. For example, Sodemann et al. (2008a) investigated interannual winter precipitation variability over Greenland by determining the sources of water vapor using a Lagrangian model. They found strong moisture source variability related to variability in the large-scale circulation, which has important implications for the interpretation of stable isotopes in ice cores (Sodemann et al. 2008b). On the global scale, Gimeno et al. (2013) used a Lagrangian model to investigate the impact of changes in oceanic moisture sources on continental precipitation and found that large regions of the Northern Hemisphere are affected by changes in moisture source conditions (mainly over the central North Atlantic and subtropical western North Pacific) during boreal winter. Winschall et al. (2014) linked Mediterranean precipitation extremes with intensification of moisture source evaporation using a Lagrangian method. They found that remote moisture source regions over the North Atlantic and the European and African land surface show stronger surface evaporation prior to extreme precipitation events, whereas Mediterranean sources show no increase.

This paper develops a novel framework to attribute variations in regional precipitation to a number of physical processes. It adopts a Lagrangian frame of reference to sample temperature and specific humidity fields from the European Centre for Medium-Range Weather Forecasts (ECMWF) analyses at points along back trajectories, but it is not a Lagrangian model in the sense that it does not solve time-dependent equations along the trajectories, in contrast to Lagrangian photochemical models, for example (Pugh et al. 2012). In the reanalysis system, temperature, winds, and humidity are evolved on the fixed grid of the ECMWF forecast model, constrained by global observations using data assimilation (Dee et al. 2011).

A key difference from the Lagrangian approaches cited above lies with the identification of the ''origin location'' for air masses influencing precipitation and the way in which the two are linked. The ''origin'' is here defined as the location where the humidity mixing ratio of the air mass last increased through mixing before arrival. The subsequent precipitation only depends on the moisture carried by the air mass and its trajectory after this time. An equation relating precipitation rate to vertical motion for saturated air masses is given in section 2d. The connection between the airmass properties at this origin point and the underlying surface is assumed to be rapid (i.e., boundary layer mixing time scale is fast compared with the interval between analyses) so that the history before the ''origin time'' is not relevant. In essence, it is equivalent to stating that the sources of individual water molecules within an air mass are not important for precipitation amount, only the maximum humidity mixing ratio and the subsequent history of saturated ascent, condensation, and mixing. This approach is somewhat similar to Gustafsson et al. (2010), who studied the atmospheric moisture transport for extreme summer precipitation events in Sweden. Their origin region identification technique is based on the last cycle of humidity uptake prior to arrival over the target region [see Gustafsson et al.'s (2010) Fig. 4 for definition].

This differs from other recent trajectory studies (e.g., Sodemann et al. 2008a; Martius et al. 2013), where moisture uptake regions along trajectories associated with surface evaporation are estimated. This is necessary if investigating the source of water molecules evaporating from the underlying surface. When investigating precipitation variability, an advantage of the approach in this paper is that there is no need to follow back trajectories into the boundary layer or make assumptions regarding subgrid-scale boundary layer mixing and its influence along trajectories. The humidity field in the reanalysis is determined by the resolved flow and parameterization schemes of the ECMWF model.

Section 2e gives a more detailed evaluation of the origin definition.

Monthly precipitation amounts P are linked to physical processes that describe airmass moisture content and its loss through condensation following trajectories arriving over a target region (section 2). The processes are hypothesized to be related through five distinct multiplicative factors:

$$P \propto \mathrm{ST} \times \mathrm{LOC} \times \mathrm{AI} \times \mathrm{AF} \times \mathrm{NT}. \quad (1)$$

Quantitative factors are developed and the completeness of the factorization investigated using trajectory-based metrics in section 4. Two factors (surface temperature ST and origin location LOC) are related to the origin locations of precipitating air masses. Factor ST quantifies the direct thermodynamic influence of surface temperature anomalies (via the Clausius–Clapeyron relation) on the water vapor mixing ratio of the marine boundary layer at origin locations and hence the mixing ratio of air leaving the boundary layer, which, via moisture transport along the trajectory, influences the precipitation totals. Factor LOC quantifies the impact of varying the origin locations while supposing that the surface temperature field is fixed, thereby capturing the impact of variations in large-scale transport for a given map of surface conditions.

The three remaining factors are related to the ascent of air masses, which is necessary for condensation and formation of precipitation. The moisture release can be altered by the rate of ascent over the target region (ascent intensity AI), the mass of ascending air over the region (ascent mass fraction AF), and the number of analyses in a given period producing precipitation NT. For regions strongly affected by cyclones in a storm track, this last factor is hypothesized to be related to cyclone variability via the number of cyclones CC and their average duration over the target region CD.

The physical factors influencing monthly precipitation variability in the U.K. summer season are examined using ERA-Interim reanalysis data (1979–2013) and the independent rain gauge estimate of England and Wales precipitation (EWP). The study region is chosen because of the quality and length (since 1931) of the daily EWP time series (Alexander and Jones 2000), together with the influence of the North Atlantic storm track on the United Kingdom. Summer is chosen because of the anomalous 5- and 10-day precipitation totals that have occurred during this season over the last decade (de Leeuw et al. 2016). Section 2 will discuss the data and methodology developed to investigate precipitation variability using the Lagrangian framework. Section 3 investigates the airmass origin locations and their variability. Section 4 introduces the factorization used to investigate precipitation variability, which is applied to the England and Wales region in section 5. Section 6 presents a summary and discussion of the main results.

2. Data and trajectory methodology

a. Observations: England and Wales precipitation

The EWP daily dataset, which is maintained and updated by the Met Office Hadley Centre (www.metoffice.gov.uk/hadobs/hadukp/), is a spatial average of individual rain gauge observations over the England and Wales region (Alexander and Jones 2000). It constitutes one of the longest statistically homogeneous daily precipitation datasets available (1931–present). The EWP estimate is based on the weighted contribution of five climatologically different subregions (Wigley et al. 1984; Wigley and Jones 1987). In each region, 7–15 evenly distributed stations (depending on the available data; see Alexander and Jones 2000) determine the precipitation for the region. Each rain gauge is scaled by its corresponding regional monthly climatology so that the regional data are not weighted toward sites with locally high precipitation (e.g., because of local orographic effects). This scaling allows varying gauge configurations (because of changing observation networks) to be combined to produce a robust and homogeneous time series.

b. Back trajectory calculations using ECMWF reanalyses

The Reading Offline Trajectory (ROTRAJ) model calculates back trajectories following the resolved flow in atmospheric reanalyses (Methven 1997; Methven et al. 2003) from the ECMWF. The ERA-Interim reanalysis is used here, which is based on the ECMWF IFS model [Cy31r2; Dee et al. (2011) and references therein]. The analysis has a spectral horizontal resolution of T255 and 60 vertical levels (top at 0.1 hPa). The ROTRAJ model takes the full-resolution spectral data on model η levels and transforms temperature, vorticity, horizontal divergence, and surface pressure to obtain horizontal winds, temperature, and the vertical velocity in η coordinates on a Gaussian grid. Specific humidity is evolved on the same grid without spectral transformation. The velocity at each trajectory point is interpolated from the 3D velocity field of the analysis, using linear interpolation in time and horizontal directions and cubic interpolation in the vertical direction. The 3D trajectory equation (in the terrain-following η coordinates) is integrated using a fourth-order Runge–Kutta scheme with six time steps over the 6-h interval

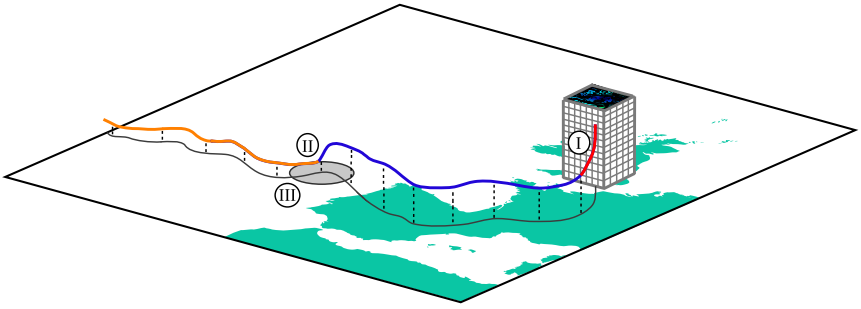

FIG. 1. An illustration of the RDF3D technique. This technique calculates back trajectories from a dense arrival grid using the resolved flow from a model, of which the colored line in the schematic is an example. Also shown are the three important factors for determining the impact of the origin location on the precipitation variability: the relation between changes in specific humidity and precipitation at the arrival region (I; red part of trajectory), the location of the origin region (II), and the connection with the surface at the origin region (III). The origin is defined as the location where the moisture content of the air mass is last modified by moistening before arrival. Therefore, the orange part of the trajectory does not influence the results presented in this paper.

between analyses. At every trajectory position (longitude, latitude, and pressure), four attributes (temperature, specific humidity, height, and boundary layer height) are interpolated from analysis fields and stored every 6 h along back trajectories. Note that boundary layer height (BLH) is a forecast model product. Data were retrieved for each boreal summer month (JJA) from 1979 to 2013, giving 35 yr of data.

Back trajectories were calculated from a dense 3D "arrival" grid positioned over the United Kingdom: 0.25° × 0.4° (≈28-km resolution) with 32 equally spaced pressure levels between 975 and 200 hPa, such that each point is associated with a box of approximately equal mass (Fig. 1). The domain spans the England and Wales region (50.6°–54.5°N, 4.5°W–0.7°E). A total of 6240 trajectories are released from the grid every 6 h and integrated backward for 8 days. Throughout the 35-yr ERA-Interim period, this amounts to 80.4×10^6 trajectories. Work by James et al. (2004) and Gustafsson et al. (2010) showed that 8-day trajectories are sufficient to determine the airmass origin regions for precipitation in Europe. It will be shown later that 8-day trajectories are also able to identify origins for all but 3% of trajectories precipitating over the England and Wales region.

The reverse domain-filling 3D trajectory (RDF3D) technique (Methven et al. 2003) described above is able to capture the humidity structure of air masses associated with cyclones and their attendant fronts over the region, as illustrated for summer 2007 by Blackburn et al. (2008). Methven et al. (2003) compared the ROTRAJ model with aircraft observations over the United Kingdom and found that RDF3D calculations using ECMWF analyses were able to simulate humidity structures accurately with widths as narrow as 30 km because of the tracer-scale cascade effects of stirring by the large-scale straining flow (Methven and Hoskins 1999).

c. *The ROTRAJ precipitation estimate*

A key aim of the Lagrangian method is to quantify the contribution to precipitation from each trajectory arriving on the 3D grid and to relate that precipitation to airmass characteristics. The following three sections relate to the stages I, II, and III along trajectories illustrated in Fig. 1. Section 2c describes stage I—the estimate of precipitation based on changes in specific humidity along trajectories over the final 6 h. Section 2d describes the link between moisture at the origin location (II) and precipitation in stage I. Section 2e links the moisture at the origins (II) to the properties of the underlying surface (III).

Condensation over the region is captured in terms of a specific humidity decrease along each individual trajectory (subscript k):

$$\Delta q_k = q_k(0) - q_k(-t), \tag{2}$$

where $q_k(0)$ and $q_k(-t)$ are the specific humidity at the "arrival time" and at interval t before arrival, respectively. A 6-h interval is selected: this is the separation of analyses in ERA-Interim and is sufficiently short that air parcels do not typically move far relative to the scale of the arrival domain so that any precipitation can be considered to be over the domain. Changes in specific humidity along the trajectory are related to either condensation ($\Delta q_k < 0$), evaporation ($\Delta q_k > 0$), and/or mixing (Δq_k of either sign). When $\Delta q_k < 0$, the

contribution of that trajectory to precipitation is $p_k = m_k \Delta q_k$, where m_k represents the arrival gridbox mass.

Summing downward from the top of a grid column (k increasing), at each level, the vertically integrated precipitation contribution, denoted as P_k, is calculated as

$$P_k = P_{k-1} - m_k \Delta q_k, \tag{3}$$

looping over k from $P_0 = 0$. When $m_k \Delta q_k > 0$ and is also larger than the condensate integrated above that level ($m_k \Delta q_k > P_{k-1} > 0$), it is assumed that all the condensate from above is lost through dry air mixing and evaporation (i.e., reset $p_j = 0$ for $j \leq k$ and $P_k = 0$).

In the case of partial evaporation of condensate at level k (i.e., $P_{k-1} > m_k \Delta q_k > 0$), the contribution to precipitation of all trajectories above the evaporating layer ($j < k$) is adjusted by a constant fraction, using

$$p_j = -m_j \Delta q_j \left(1 - \frac{m_k \Delta q_k}{P_{k-1}}\right). \tag{4}$$

This redistribution does not change the vertically integrated precipitation P_k. Within the boundary layer ($z < z_{\mathrm{BL}}$), all trajectories where $\Delta q_k > 0$ are assumed to be influenced by evaporation of moisture from the surface and are therefore not included in the precipitation calculation Eq. (3).

Descending air masses (increasing pressure) move to higher temperature and saturation vapor pressure, so moisture is not expected to condense. Therefore, descending trajectories with $\Delta q_k < 0$ are assumed to be mixing with drier air and do not contribute to the surface precipitation estimate. Hence, only trajectories ascending upon arrival will be considered when calculating the surface precipitation.

Finally, the surface precipitation P_s for each column is given by $P_s = \sum_{j=1}^{N} p_j$, where p_j is the precipitation contribution for individual ascending trajectories after the adjustments described above. Note that P_s would equal P_k at the bottom of the column if it were not for the evaporation in the boundary layer and the exclusion of contributions from descending trajectories.

Here, the ROTRAJ estimate of daily precipitation is compared with EWP observations and ERA-Interim forecasts for all summers (JJA) between 1979 and 2013, using a ranked comparison of all daily precipitation estimates (Fig. 2). The largest discrepancy is for light precipitation events ($<4\,\mathrm{mm\,day^{-1}}$) where the ROTRAJ estimate is too large by 58% relative to EWP. Excluding these light precipitation events, the best linear fits with EWP are similar. The linear regression has a slope 0.77 ± 0.005 for ROTRAJ, versus 0.78 ± 0.005 for ERA-Interim, indicating that the ROTRAJ estimate is lower than observations by the same factor as the underlying ECMWF model precipitation. Comparison of the PDFs

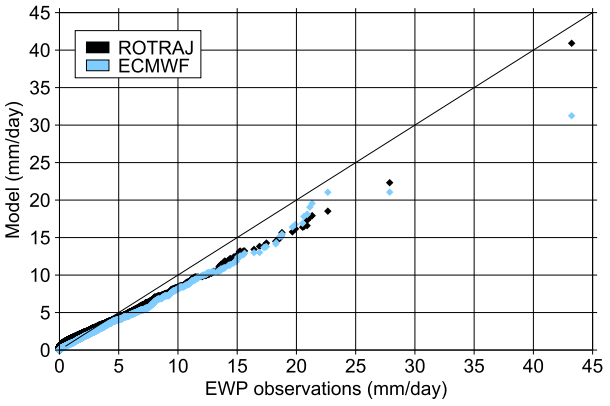

FIG. 2. Comparison of the ranked daily precipitation estimate (1979–2013) between EWP and the ROTRAJ (black line) estimate (only ascending trajectories are included). The ECMWF model estimate (blue line/dots) is also compared with EWP. Both models underestimate the observations by a similar amount (23%), apart from the light precipitation ($<4\,\mathrm{mm\,day^{-1}}$) events where the ROTRAJ estimate is too large. For wet events ($>4\,\mathrm{mm\,day^{-1}}$), both models have similar skill.

of precipitation rates for ECMWF and ROTRAJ (not shown) reveals that both are indistinguishable from a Weibull fit to the EWP observations aside from a uniform scaling factor of 0.77 (de Leeuw et al. 2015). This demonstrates consistency between the back-trajectory calculation and the evolution of moisture in the ERA-Interim analysis. The Spearman rank correlation coefficient between the time series of ROTRAJ with EWP observations ($R^2 = 0.76$) is also similar to correlation between ERA-Interim forecasts and EWP ($R^2 = 0.78$).

d. *The relation between humidity at origin locations and precipitation over the arrival region*

The aim in this section is to relate precipitation rate at any point along a trajectory to the moisture at the origin location (to be defined in section 2e). Since saturation vapor pressure is a function of temperature T only [$e_s(T)$ is given by the Clausius–Clapeyron relation], the saturation specific humidity q_s is a function only of pressure p and temperature. Moreover, the thermodynamic state of a saturated air parcel is described by only two independent variables. Therefore, we can consider the equivalent potential temperature at saturation θ_{es}, as a function of q_s and p only, and its total derivative can be written without approximation as

$$d\theta_{\mathrm{es}} = \left.\frac{\partial \theta_{\mathrm{es}}}{\partial p}\right|_q dp + \left.\frac{\partial \theta_{\mathrm{es}}}{\partial q}\right|_p dq. \tag{5}$$

Now consider the rate of change along a trajectory within a saturated air mass. Since $D\theta_{\mathrm{es}}/Dt = 0$ in the absence of mixing, Eq. (5) reduces to

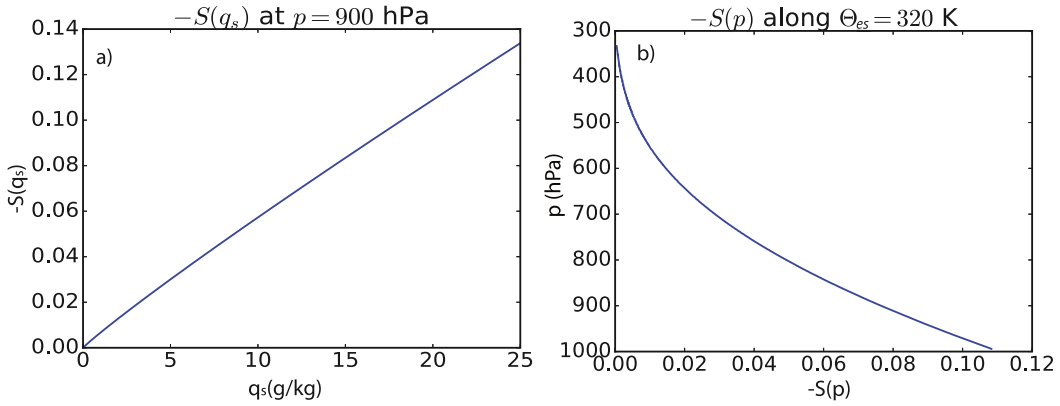

FIG. 3. Thermodynamic function $S(p, q_s)$ for (a) a constant pressure level $p = 900$ hPa and (b) along a moist adiabat with equivalent temperature $\theta_{es} = 320$ K.

$$R = \frac{\omega}{p_0} S(p, q_s), \tag{6}$$

where $R = -Dq/Dt$ is the condensation rate and $\omega = Dp/Dt$ is the vertical velocity in pressure coordinates. The quantity p_0 is a constant used to nondimensionalize $S(p, q_s)$, which is the thermodynamic function

$$S(p, q_s) = p_0 \frac{\partial \theta_{es}}{\partial p}\bigg|_q \bigg/ \frac{\partial \theta_{es}}{\partial q}\bigg|_p . \tag{7}$$

Equation (6) encapsulates a physical basis for a partition of precipitation rate between thermodynamics (the invariant function S) and the dynamics through the vertical motion ω (O'Gorman and Schneider 2009). The partition is dependent on using the Lagrangian frame. Since each trajectory follows a different path (p, q_s), the thermodynamic influence is implicitly dependent upon the path. Also, the vertical motion depends on the coupling between the momentum and thermodynamic equations. Despite these complexities, we use this Lagrangian framework to identify different physical mechanisms influencing precipitation variability.

In Fig. 3a, the function $S(p, q_s)$ is shown holding the pressure constant at 900 hPa. The empirical formula of Bolton (1980) is used to define θ_{es} in the numerical calculations. The function S is almost linearly dependent upon q_s. This implies that if humidity at low-level origins is varied, the precipitation rate is expected to scale with the origin humidity in Eq. (6) (if the trajectory pathway can be taken as unchanged). Figure 3b shows the variation of S as pressure decreases following a moist pseudoadiabat during saturated ascent. It illustrates how the greatest proportion of condensation must be associated with ascent at the lowest levels (highest pressure). Nevertheless, the key point is that the curve is known given only the value of θ_{es}, and all adiabats give a similar-shaped monotonic variation in S with p. Therefore, in section 4a, it will be assumed that a fractional increase in specific humidity at the origin would result in a proportionate increase in precipitation along a trajectory. This relies only on $S(p, q_s)$ being a known monotonic function of q_s and an assumption of weak mixing.

The integral of Eq. (6) along trajectories yields $\delta q = X \times \delta p/p_0$. The variable X is not known in general since $S(p, q_s)$ is nonseparable and one cannot evaluate the integral analytically. However, a compact nonlinear relation is expected between δq and δp if trajectories originate from a similar pressure level and experience saturated ascent. This prediction is tested for the trajectories calculated from analyses using a number density plot of $[p_{origin} - p(6\,h)]$ versus $[q_{origin} - q(6\,h)]$ for all trajectory origins identified as last exit from the boundary layer (called "CAT I" in section 2e). It shows a reasonably compact relation (linear correlation $R = 0.83$) between the two quantities (Fig. 4), indicating that the Eq. (6) holds to some extent following the flow resolved in the reanalyses between origin (location II in Fig. 1) and the start of the saturated ascent over the last 6 h (phase I). The effects of mixing and different origin pressures smear the relation out. Note that this means that although mixing occurs, the precipitation along the trajectory scales with q_{origin}.

e. Determining the trajectory origin locations

In section 1, the airmass origin was introduced as the location where the water vapor mixing ratio last increased related to mixing. It will be shown that this occurs most often at the point of exit from the boundary layer (BL). However, to specify the precise origin

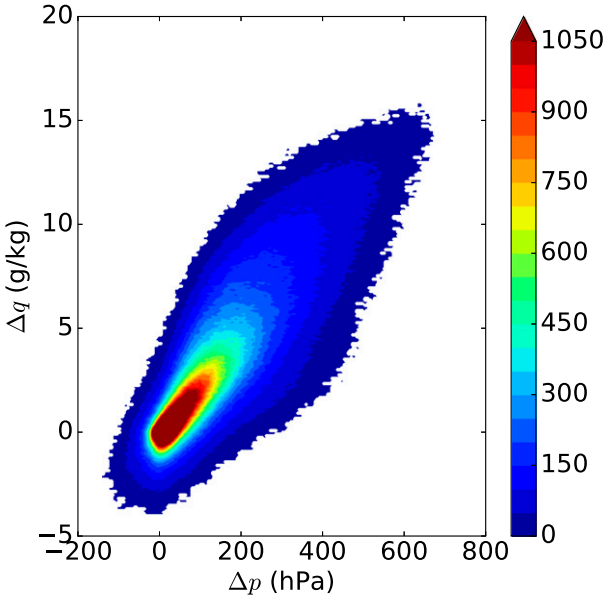

FIG. 4. A number density plot of the change in pressure between the origin location and $t = -6$ h at the start of the precipitation calculation [$p_{\text{origin}} - p(-6\,\text{h})$] vs the change in specific humidity between the same time points [$q_{\text{origin}} - q(-6\,\text{h})$]. The calculations are based on CAT I trajectories only.

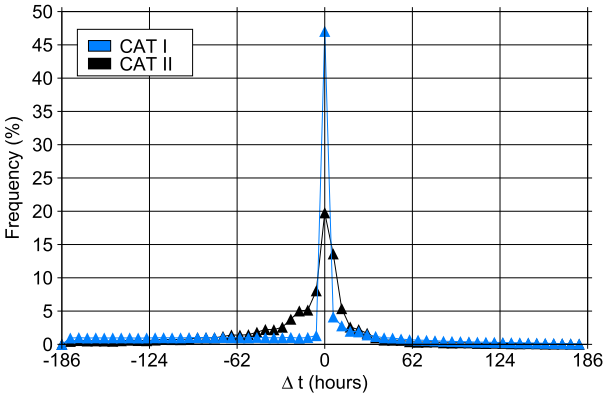

FIG. 5. Relative frequency histogram of the difference between the time determined for the origin location and time of maximum specific humidity (q). Results are shown for CAT I origins (blue line/points, well-mixed turbulent BL) and CAT II origins (black line/points, partially mixed moist convective layer) separately. Negative times indicate a maximum specific humidity that occurs later (closer to the arrival time) than the point labeled as origin.

locations, it is necessary to consider boundary layer type and the implications for mixing of moisture.

The first criterion used to define a trajectory origin point is based on the last exit of the BL as defined by the ECMWF forecast model. The BL height diagnostic identifies the height of the well-mixed turbulent boundary layer. In unsaturated conditions, this coincides often with an inversion. However, in moist convective boundary layers capped by cloud, it identifies the top of the well-mixed subcloud layer, not the partially mixed cloud layer above. If a trajectory is below z_{BL} at any time, the last exit from the BL is identified as the origin location, and the trajectory is described as CAT I.

In unsaturated conditions, the virtual potential temperature θ_v (including molecular mass effects of water vapor loading) becomes well-mixed, and the mixing line between the surface and BL top (Emanuel 1994) is used to isolate the influence of surface temperature variability on trajectory humidity.

A second criterion is necessary to identify trajectories originating from the cloud layer of moist convective boundary layers but that do not stray below z_{BL} at any point. These will be described as CAT II origins. The criterion is based on the last significant increase in equivalent potential temperature θ_e along the trajectory, as this is a conserved quantity following saturated or unsaturated air masses in the absence of mixing. Typically, air leaving the BL, for example, in a warm conveyor belt flow, possesses θ_e that is greater than its surroundings. Consequently, θ_e can only decrease through mixing and radiative cooling after exit (e.g., Methven et al. 2003). Therefore, any significant increase in θ_e is attributed to mixing within the cloudy BL or a region of deep convection. The Intercontinental Transport and Chemical Transformation (ITCT) Lagrangian experiment in 2004 used aircraft to intercept the forecast trajectories of air masses at locations spanning the North Atlantic. Methven et al. (2006) showed that in Lagrangian cases (avoiding regions of convective mixing), the observations by multiple aircraft connected by airmass trajectories revealed matching chemical fingerprints (indicating that it was indeed the same air mass), and the θ_e agreed to within 2 K on average between the analyses and observations at those locations. Therefore, to be certain to not sample model errors, the threshold defining a CAT II origin is a θ_e increase exceeding 2.5 K. Using this θ_e threshold does not exclude mixing in very stably stratified regions with drier air above the trajectory air mass. Therefore, increases in θ_e must be accompanied by an increase in q to ensure they represent moistening of the trajectory.

The fraction of the ROTRAJ precipitation estimate associated with CAT I origins is 70%, CAT II origins 27%, and trajectories with no origin within 8 days contribute 3%. This small percentage of unidentified origins justifies the 8-day limit for back trajectories used in this study.

Figure 5 compares time of last exit from the BL (selected using CAT I or CAT II origin) with the time of observed maximum specific humidity along each contributing trajectory (using the whole dataset). The

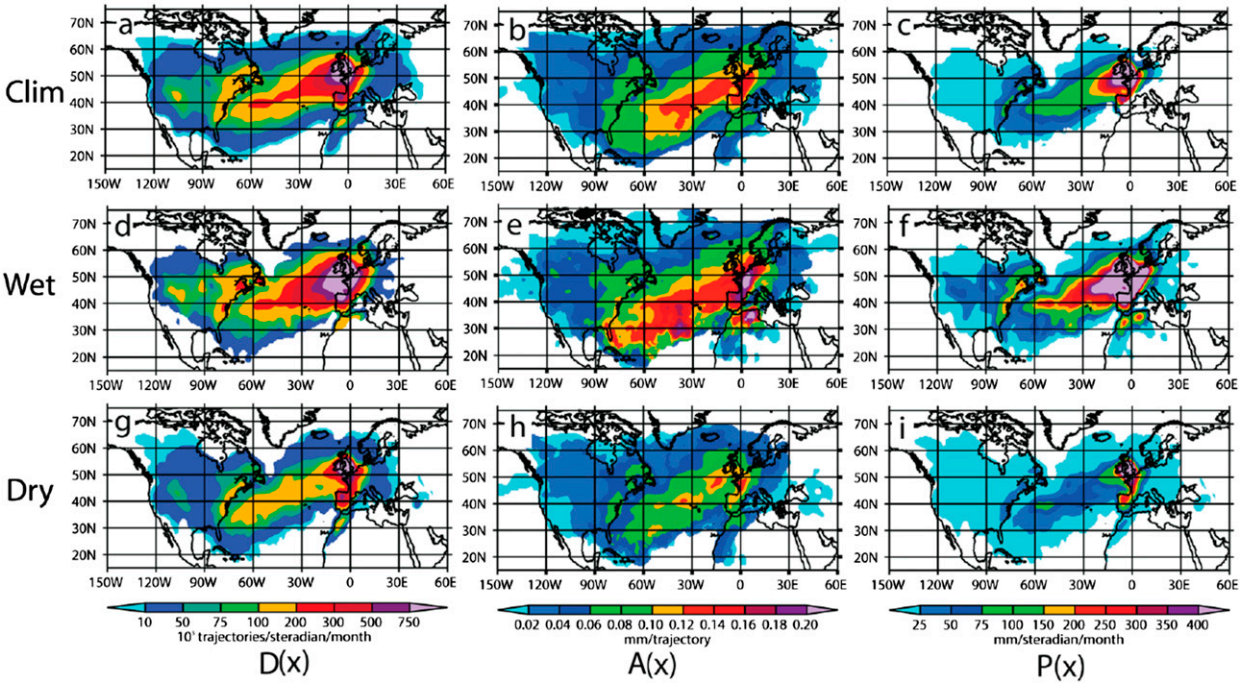

FIG. 6. Origin maps for (top) the climatological period and for the (middle) wet and (bottom) dry composites, consisting of (left) a map for the trajectory origin number density per month $D(\mathbf{x})$, (center) the average precipitation contribution per trajectory $A(\mathbf{x})$, and (right) the total precipitation contribution per month $P(\mathbf{x}) = D(\mathbf{x}) \times A(\mathbf{x})$.

resulting histogram shows that the definition used for the origin location coincides with the key location where the maximum moisture content of each trajectory air mass is set. The tighter peak for CAT I trajectories in Fig. 5 indicates a stronger link between the cessation of BL mixing and maximum humidity in those cases.

3. Trajectory origins and their variability

The number density map of trajectory origins can be estimated as

$$D(\mathbf{x}) = \sum K(\mathbf{x}_j), \tag{8}$$

where $K(\mathbf{x}_j)$ is a kernel function at the origin position of each trajectory $\mathbf{x}_j$ that arrives over the target region. The kernel is defined in spherical coordinates, following Hodges (1996), by a parabolic function with radius of 200 km, sufficient to obtain a smooth density map over the Atlantic from approximately 10^5 trajectories per month. The global integral of $D(\mathbf{x})$ equals the total number of contributing trajectories.

A map of origin-average precipitation contribution $A(\mathbf{x})$ [mm (trajectory)$^{-1}$] is obtained following the technique of Methven et al. (2001) by weighting each trajectory with the corresponding precipitation contribution p_j [defined by Eqs. (2)–(4)]:

$$A(\mathbf{x}) = \frac{\sum K(\mathbf{x}_j) p_j}{D(\mathbf{x})}. \tag{9}$$

The total contribution of each origin location to the target region precipitation is given by

$$P(\mathbf{x}) = A(\mathbf{x}) \times D(\mathbf{x}). \tag{10}$$

Integrating $P(\mathbf{x})$ over the globe results in the total monthly ROTRAJ estimate of precipitation over the target region. This method will now be applied to the England and Wales region.

a. Climatology

The number density map[1] for origins of trajectories arriving over England and Wales, $D(\mathbf{x})$, is shown in Fig. 6a. The maximum density of origins is over the England and Wales region itself, but a large fraction of the trajectories originates to the southwest of the United Kingdom over the North Atlantic Ocean, related to moisture transport by cyclones in the storm track. Local maxima are also found along the coasts of North

[1] The results are rescaled to represent the number of trajectories per steradian. For Earth, 10^5 trajectories per steradian corresponds to approximately 1 trajectory per 10 km^2.

America and North Africa. These are related to the deeper boundary layers over land in daytime compared to the ocean boundary layer. Trajectories can exit the boundary layer horizontally moving from land to ocean (e.g., Peake et al. 2014).

The origin-average precipitation contribution per trajectory $A(\mathbf{x})$ is shown in Fig. 6b. Typically, the precipitation falling in the last 6 h before arrival (over the target region) is much smaller than the net condensation along the trajectory, $[q_{\text{origin}} - q(0)]$, because a fraction of the origin humidity q_{origin} is lost through condensation and precipitation earlier along the trajectory. Trajectories originating over the Atlantic Ocean southwest of the United Kingdom contribute most on average to precipitation over England and Wales. There is a tendency for more precipitation to be associated with trajectories originating farther south, which is related to the higher temperatures in those regions (and therefore higher saturation vapor pressure and more BL moisture).

The product of Figs. 6a and 6b gives the total precipitation contribution (Fig. 6c). The maximum occurs over the United Kingdom, while the importance of trajectories originating from North America is decreased because of their small individual contribution to precipitation over England and Wales. Trajectories over the Atlantic basin southwest of the United Kingdom dominate the ocean origin contribution to England and Wales precipitation.

b. Composites of wet versus dry months

Composite plots are created for the 10 wettest and driest summer months in the EWP observational dataset. Changes in density of origin $D(\mathbf{x})$, are mainly associated with the number of precipitating trajectories over the arrival region. Comparing Figs. 6d and 6g, more than double the number of trajectories originate over the Atlantic Ocean in the wet composite. The trajectory origin density from the European continent is also higher but does not change in shape, with a peak over northern Spain and large parts of western France.

The origin-average precipitation per trajectory $A(\mathbf{x})$, also differs markedly between wet and dry months (Figs. 6e and 6h). This includes the effects of both the changes in origin moisture content and changes in ascent at arrival. Again, the highest origin-average precipitation contribution in the wet composite originates over northwest France.

Multiplying these two fields gives the total precipitation contribution $P(\mathbf{x})$, in Figs. 6f and 6i. Comparing the two extreme composites with climatology (Fig. 6c), the largest changes are observed over the Atlantic Ocean to the southwest of the United Kingdom.

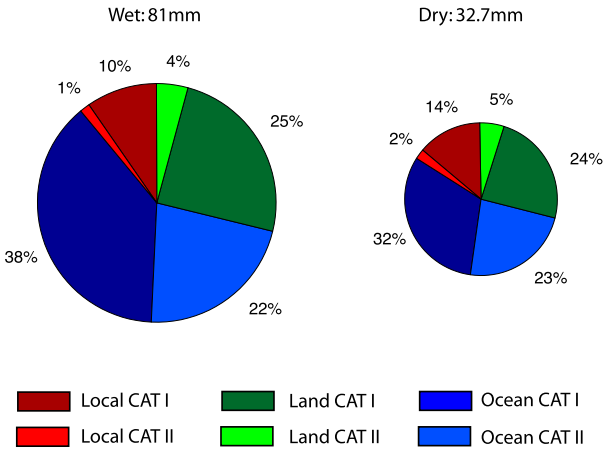

FIG. 7. The partial contribution of the local region (red), other land regions (green), and the ocean (blue) to the EWP. The dark and light colors represent the contribution of the CAT I and CAT II trajectories, respectively. The diagrams show the (left) wet and (right) dry composites, each consisting of the 10 most extreme months. The area of both diagrams is scaled to represent the total precipitation for each composite.

This indicates that a large fraction of the precipitation variability is related to air masses originating from this region.

c. Ocean and land origin regions

Integrating the total precipitation contribution $P(\mathbf{x})$ separately over the ocean, land, and local (England and Wales) regions gives the partial contribution of each region to the total ROTRAJ precipitation estimate for the wet and dry composites (Fig. 7). The total precipitation is almost 3 times higher in the wet relative to the dry composite.

The relative contributions of the three regions are broadly similar in the wet and dry composites, with over half of the precipitation having an oceanic origin. Despite the highest origin number density over England and Wales, the small area results in a small total contribution (≈11% in wet and 16% in dry months). The main difference between the wet and dry composites is a larger contribution of ocean origins in the wet composite, which is replaced by a larger local contribution in the dry composite. The relative contribution of other land regions is unchanged.

The partition between CAT I and CAT II origins in Fig. 7 reveals that the land and local origin regions are dominated by CAT I (the turbulent boundary layer), while the ocean has a relatively large contribution from CAT II (the cloud layer capping the convective marine BL).

Differences between the wet and dry composites in the precipitation contributions imply systematic

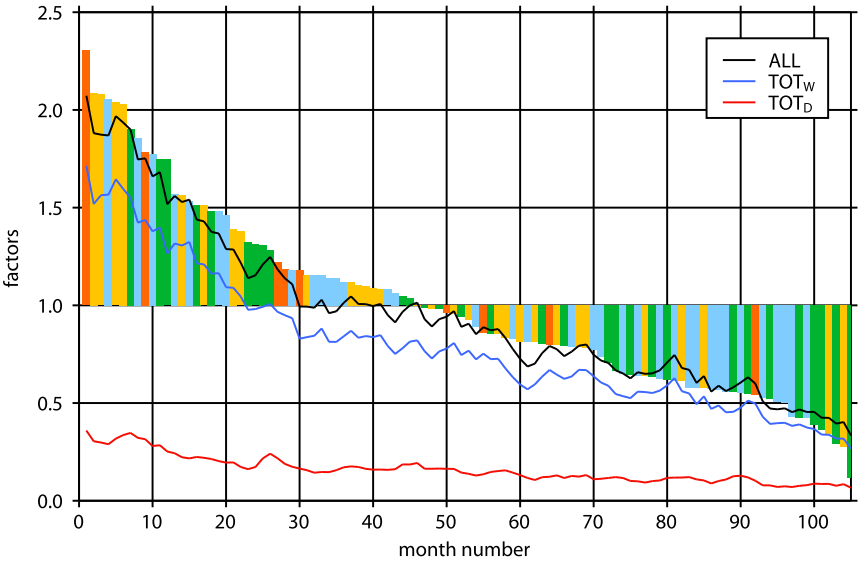

FIG. 8. The ranked monthly EWP observations for JJA 1979–2013 (bars) and the summed impact for the wet and dry analyses and their combination (lines). The fractional contribution of the wet and dry analyses in each month are normalized relative to the climatological average precipitation. The colors of the bars indicate the decade of the month (blue is 1979–89, green is 1990–99, yellow is 2000–09, and red is 2010–13), showing that most of the wettest months occurred after 2000. To reduce noise, a 5-point running average is applied to the wet (blue) and dry (red) contributions and their combination (black).

differences in the large-scale circulation and the characteristics of cyclones in the North Atlantic storm track. This could involve a combination of the number of cyclones, their intensity, and tracks. The consideration of all the factors outlined in the introduction [Eq. (1)] will allow a more specific attribution of precipitation changes to individual mechanisms.

4. Factorization of precipitation variability into physical mechanisms

Five factors are hypothesized to dominate precipitation variance, as introduced in section 1. First, the dataset is partitioned into "dry" (subscript d) and "wet" (subscript w) analyses because the statistics of these two subsets are very distinct. Wet analyses are defined by a threshold of 1-mm precipitation accumulation (for the England and Wales average) over the 6 h prior to each analysis using the ROTRAJ estimate. Figure 8 shows a histogram of EWP ranked from wettest to driest months, with the separate contributions to the ROTRAJ estimate from the wet analyses (TOT_w), the dry analyses (TOT_d), and their total. All monthly values are normalized by the climatological mean EWP, and the trajectory estimates have been divided by the appropriate scaling (0.77) to account for the underestimation of EWP by ROTRAJ. To reduce noise, a 5-point running mean is applied to the ranked wet and dry contributions. Figure 8 shows that ROTRAJ is able to explain most of the observed summer EWP variability (approximately 88% without the running mean) and that the majority of the variability is related to the wet analyses. Therefore, the remainder of the paper will focus on the monthly precipitation estimate using the wet analyses only, P_w. This may be partitioned into three metrics:[2]

$$P_w = \overline{p}_w \times M_w \times n_w, \tag{11}$$

where $\overline{p}_w$ represents the monthly average of precipitation contribution per trajectory during wet analyses [Eq. (4)]; M_w is the average number of ascending trajectories precipitating per wet analysis, proportional to the mass of ascending air in the arrival domain; and n_w is the number of wet analyses in the month.

The time series of each term in Eq. (11) is calculated as a fraction of its climatological mean (Fig. 9). The variability in n_w clearly dominates (r = 0.81–0.90). The other two metrics ($\overline{p}_w$ and M_w) are less variable, with some interesting exceptions (e.g., August 1986). Therefore, most of the monthly precipitation variability observed over

[2] The subscript w will be implicitly assumed in the remainder of this paper unless stated otherwise.

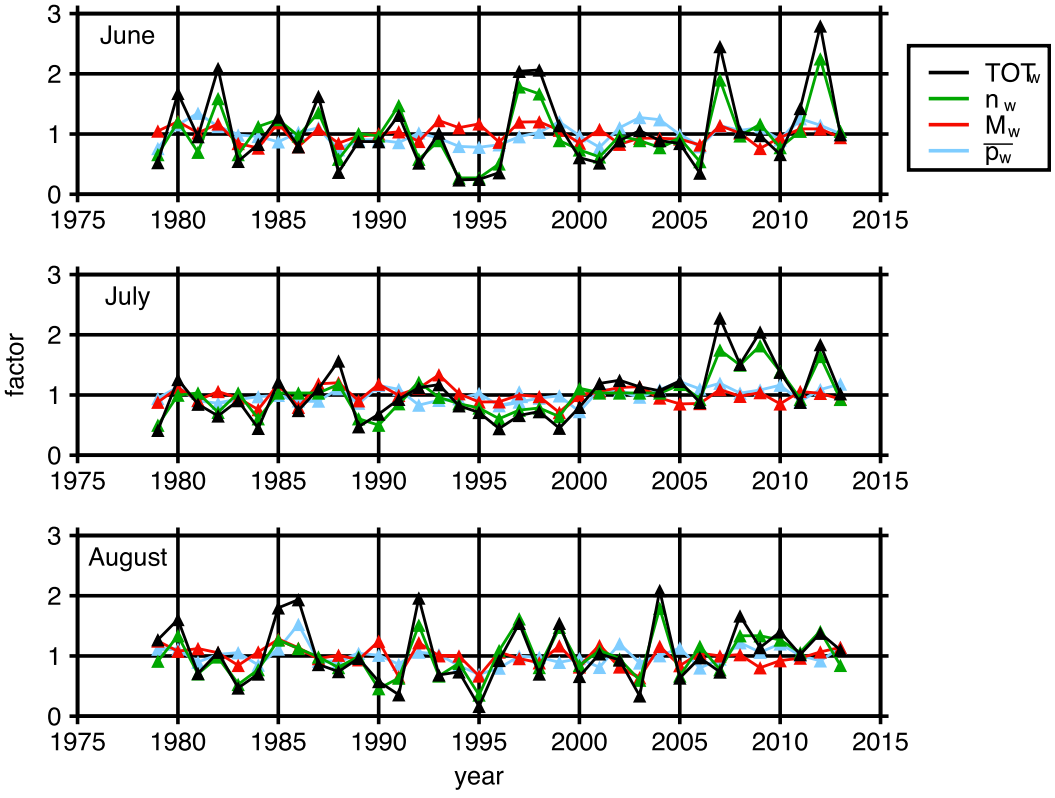

FIG. 9. Monthly variations between 1979 and 2013 for the three ROTRAJ precipitation metric terms in Eq. (11) for the wet analysis type; n_w is the total number of wet analyses (green), M_w (red) is the average number of ascending trajectories precipitating per wet analysis, and $\overline{p}_w$(cyan) is the average precipitation contribution per trajectory for the wet analyses. Values are calculated as ratios relative to the climatological average. The black line represents the combined precipitation variability in the ROTRAJ model for the wet analyses.

England and Wales can be related to the total number of analyses that exceed the wet analysis threshold [1 mm $(6\,\mathrm{h})^{-1}$].

The partition of monthly precipitation in Eq. (11) is closely related to the trajectory origin metrics defined in Eqs. (8) and (9) as follows:

$$\overline{p}_w = \int A(\mathbf{x})\,d\mathbf{x} \quad \text{and} \quad M_w \times n_w = \int D(\mathbf{x})\,d\mathbf{x}, \quad (12)$$

showing that $A(\mathbf{x})$ is related to the monthly average precipitation contribution per trajectory, while $D(\mathbf{x})$ is related to the total number of contributing trajectories. Using the trajectory model metrics in Eq. (11), it is now possible to partition the precipitation variability into multiplicative factors associated with distinct physical processes,

$$P_w = P_{\mathrm{clim},w} \times \mathrm{ST} \times \mathrm{LOC} \times \mathrm{AI} \times \mathrm{AF} \times \mathrm{NT}_w \quad (13)$$

where $P_{\mathrm{clim},w}$ is climatological average of "wet day" monthly precipitation, $\mathrm{NT}_w = n_w/\langle n_w \rangle$ the anomalous number of wet analyses, and $\mathrm{AF}_w = M_w/\langle M_w \rangle$ the anomalous ascent mass fraction (i.e., variations in the mass of ascending air over the region). The angle brackets denote the time average over the entire dataset. The $\overline{p}_w$ factor is factorized into three mechanisms that are hypothesized to dominate its variability: ST, the impact of anomalous surface temperatures at the origins; LOC, the impact of variability in origin locations; and AI, the ascent intensity. The impact on precipitation variability is calculated by changing one variable and keeping all other factors constant. By definition, the climatological average of each factor is unity.

a. ST variability

The ST factor quantifies the impact of surface temperature variations at the trajectory origins on moisture content and thence on precipitation contribution per trajectory $\overline{p}_w$. It is calculated by substituting surface temperature T_s at each origin location with its climatological value. The assumption is that affects the trajectory moisture content through the increase in saturation vapor pressure, which then scales the moisture loss

through condensation in the arrival region, holding all else equal. It is necessary to link the surface temperature to the boundary layer moisture content, the trajectory properties at the origin location, and finally Δq_k [Eq. (2)] over the last 6 h before arrival (as outlined in section 2d).

The first key assumption is that turbulent mixing between the surface and BL top is sufficiently rapid that the humidity and temperature at the location of last exit from the BL are instantaneously connected to conditions at the surface underneath. Model studies indicate that the BL exchange time scale is of the order of hours. For example, motivated by observations from the Coupled Boundary Layer Air–Sea Transfer (CBLAST) experiment, Edson et al. (2007) and Skyllingstad et al. (2007) investigated the impact of SST variability on the structure of the boundary layer using a large-eddy simulation (LES) model. They found that the boundary layer had adjusted to near steady state after 80 min.

For CAT I trajectories, defined in section 2e, the connection between the "point of origin" within the BL and the surface is made using the conserved thermodynamic property virtual potential temperature θ_v, which is well mixed within turbulent boundary layers. Taking all CAT I cases, where back trajectories extend below z_{BL} diagnosed from the ECMWF model, it is found that θ_v at the trajectory origin heights (point II in Fig. 1) is related to air surface θ_v by a linear regression with $R^2 = 0.97$.

For the CAT II trajectories, identified with origin above the turbulent mixed layer but experiencing moistening, it is found that equivalent potential temperature, θ_e, at the trajectory origin heights is related to surface θ_e by a linear regression with $R^2 = 0.67$. This is consistent with a mixing line in a moist convective BL, but the relationship is not as tight, indicating partial mixing.

The impact of substituting the actual surface temperature at each location T_s with its climatological value, denoted by $\langle T_s \rangle$, is calculated as follows. For each individual trajectory, a revised saturation vapor pressure, $e(\langle T_s \rangle)$, is calculated using the Clausius–Clapeyron relation, which yields saturation specific humidity $q_s(\langle T_s \rangle, p_s)$. Assuming that relative humidity (RH) is unchanged in the BL enables the calculation of $\langle \theta_v \rangle$ at the surface. The observed linear regression between the surface and BL top results in a value for $\langle \theta_v \rangle$ at the height of the "airmass origin." Again assuming that the RH profile is unchanged, $\langle \theta_v \rangle(p_{\mathrm{origin}}, \mathrm{RH}, \langle q \rangle)$ can be inverted to obtain an estimate of the specific humidity $\langle q \rangle$ at the trajectory origin point. Note that the RH vertical profile is observed to vary little with time within the marine boundary layer (Stevens et al. 2007; Holloway and Neelin 2009) even though the temperature and specific humidities may vary substantially. Since the marine BL profile is typically near saturation at the top, the RH profile is tightly constrained.

Finally, the fractional change in precipitation contribution of each individual trajectory p_j over England and Wales is assumed to be equal to the ratio $q_j/\langle q \rangle_j$, derived at each trajectory origin. This approach relies on the physical argument given in section 2d and the underpinning Eq. (6). Adding the changes for all trajectory origins results in an area average precipitation factor $\mathrm{ST} = \Sigma_j p_j / \Sigma \langle p \rangle_j$. Similar calculations are applied for CAT II trajectories but using θ_e as the well-mixed BL quantity in the adjustment of the vertical profile to climatological surface conditions. More details can be found in de Leeuw (2014).

b. LOC variability

The impact of changing the origin location on precipitation, while holding all else fixed, is represented by the LOC factor in Eq. (13). This factor is calculated by substituting the origin density map (as shown in Fig. 6) from the actual month with the climatological map. First, define the total available moisture (TAM) for precipitation along trajectories as

$$\mathrm{TAM} = \int D(\mathbf{x}) \overline{q}_{\mathrm{origin}}(\mathbf{x})\, d\mathbf{x}, \tag{14}$$

where $D(\mathbf{x})$ is the trajectory number density and $\overline{q}_{\mathrm{origin}}(\mathbf{x})$ the origin-average specific humidity at a location $\mathbf{x}$, defined following Eq. (9) with q_j as the kernel weight. Assuming a constant fraction α of the total available moisture (i.e., combining all trajectories) precipitates over England and Wales gives

$$P = \alpha \times \mathrm{TAM}, \tag{15}$$

where α is a constant ($\alpha = 2.8 \times 10^{-5}\,\mathrm{mm\,kg^{-1}\,kg^{-1}}$ for JJA climatology). The LOC factor in Eq. (13) is calculated as $\mathrm{LOC} = P/\langle P \rangle = \mathrm{TAM}/\langle \mathrm{TAM} \rangle$, where $\langle \mathrm{TAM} \rangle$ is defined by Eq. (14) substituting the climatological distribution $\langle D \rangle \langle \mathbf{x} \rangle$.

c. AI variability

The AI factor is an estimate of the effect on precipitation of replacing the probability distribution of ascent rate for each month with the climatological distribution, keeping all else fixed. Assuming pseudoadiabatic displacement, a change in ascent rate of trajectories over the arrival region is related to the average decrease in specific humidity ($\overline{\Delta q_w}$) as predicted by Eq. (6).

Calculation of AI for an individual month is illustrated schematically in Fig. 10. For each trajectory, the ascent rate (net ascent in the last 6 h over the arrival region, denoted by $-\Delta p$) is known, and its percentile in

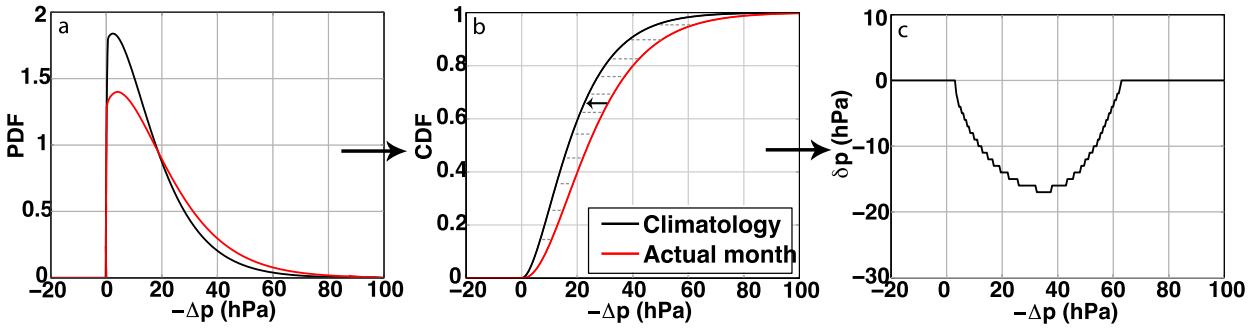

FIG. 10. Schematic illustration of the calculation of AI factor with the black lines representing climatology and the red, the actual monthly values. (a) Net ascent ($-\Delta p$) over the last 6 h of each trajectory is adjusted by comparing the PDF of monthly ascent rates with its climatology. At each value of (b) the CDF, the additional pressure change (δp) required to shift the monthly curve to climatology is calculated. (c) The change in ascent δp is then applied to each individual trajectory (given its net ascent rate $-\Delta p$) and is related to a change in condensation δq using the moist adiabatic lapse rate.

that month's cumulative distribution function (CDF) of ascent rate is found. The $-\Delta p$ is replaced by the ascent rate corresponding to the same percentile in the climatological CDF. The change in ascent rate δp (the left arrow in Fig. 10b) is used to calculate a change in condensation δq assuming a pseudoadiabatic displacement [i.e., moving along the S curve illustrated in Fig. 3b and using Eq. (6)]. More details of these calculations are given in de Leeuw (2014).

d. *Association of* NT_w *with cyclone statistics*

In midlatitude storm tracks, fractional changes in the number of wet analyses per month, NT_w, are hypothesized to be chiefly associated with cyclone activity. These variations may be partitioned into the number of cyclones passing over the region of interest (cyclone count CC) and the average time that each cyclone affects the region (cyclone duration CD):

$$NT_w \approx CC \times CD. \tag{16}$$

To test this, cyclone count and duration are estimated using Hodges' (1994) cyclone-tracking scheme. This scheme tracks maxima in 850-hPa relative vorticity fields at a 6-h frequency. The ERA-Interim reanalyses are used, truncated to a spectral resolution of T42, ensuring that vorticity maxima are associated with cyclone centers rather than fronts (Hodges 1999).

The correlation between NT_w (wet analyses per month) and the number of analyses with cyclones (CC × CD) is maximized by varying the boundaries of the domain within which cyclones are counted. The maximum correlation is found to occur for a threshold of $1\,\text{mm}\,(6\,\text{h})^{-1}$ and the domain sizes as indicated in Table 1 for each calendar month. Based on these criteria, the total number of cyclone tracks per month and their average duration within the domain are calculated and divided by their climatological average to obtain normalized factors CC and CD.

5. The factorization applied to precipitation variability for England and Wales

Now that distinct factors quantifying the variability of specific physical mechanisms have been determined, their individual and combined skill in explaining the observed precipitation variability for summer in the EWP dataset can be assessed. The combination of factors using Eqs. (13)–(16) is able to represent approximately 86% of the variance in the EWP precipitation observations (see Table 2 for related correlation coefficients), giving confidence that all the important mechanisms of the precipitation variability are captured. The Pearson correlation coefficients in Table 2 also show that the combination of all the wet factors (TOT_w column) gives a better correlation with observations than any individual factor.

a. *Relative importance of precipitation factors*

Figure 11 shows ranked monthly precipitation, as in Fig. 8, together with the total and individual contributions of the five factors for the wet analyses [Eq. (13)].

TABLE 1. The domain size within which the cyclone feature occurrence has the highest correlation with the number of wet 6-h intervals for the England and Wales regional average. The associated squared correlation R^2 and the climatological average monthly CC (average is between presented values) and CD (number of 6-h analysis intervals) are shown.

	Relevant cyclone area	R^2	CC	CD (analyses)
June	49°–61N°, 10°W–0°	0.66	5–6	3.5
July	47°–64°N, 12°–1°W	0.69	6–7	4.1
August	48°–60°N, 19°–1°W	0.65	7–8	4.6

TABLE 2. Pearson correlation coefficients r for all the factors of the ROTRAJ model related to the wet analyses in June, July, and August compared with the observed precipitation variability (EWP) between 1979 and 2013. Also included is the total wet analyses variability (TOT_w). The SD for each factor, calculated as a fraction of the climatological average (SD/mean), is scaled to account for the underestimate of 23% by the ROTRAJ model.

	EWP	TOT_w	NT	AF	AI	LOC	ST
June							
r_{EWP}	1	0.943	0.900	0.669	0.658	0.004	−0.342
SD	0.541	0.447	0.358	0.148	0.128	0.068	0.039
July							
r_{EWP}	1	0.939	0.805	0.623	0.699	0.238	−0.506
SD	0.464	0.338	0.277	0.136	0.115	0.056	0.049
August							
r_{EWP}	1	0.910	0.855	0.750	0.421	0.033	−0.462
SD	0.420	0.358	0.294	0.165	0.154	0.065	0.048

The dominant factor in the precipitation variability is simply the number of wet analyses within each individual month NT_w. The two factors related to local storm dynamics, AI and AF, also vary systematically with monthly precipitation anomalies.

The relative contribution of each factor to precipitation variability is more clearly quantified using a Taylor diagram (Taylor 2001), shown in Fig. 12. This displays factor variance and correlation with observed precipitation. Radius represents the ratio of the standard deviation (SD) of each factor to the climatological average precipitation and is a measure of the amplitude of variability. Azimuth represents the correlation coefficient between the time series of each factor and observed precipitation (1979–2013). The axis scaling is chosen so that the distance between any two points on the diagram equals their centered RMS difference (green semicircles in Fig. 12). Therefore, the skill of an individual factor is related to its distance from the "observed" variability.

Figure 12 confirms that the number of wet analyses NT_w is the dominating factor in the ROTRAJ precipitation variability, with a correlation coefficient between 0.8 and 0.9 and a standard deviation (percent of mean) between 28% and 36% for the three summer months. As shown in Table 1, this variability is dominated by cyclone statistics in the region. The second and third most important factors are the AI and AF, but their individual contributions are much smaller than NT in terms of correlation and amplitude, resulting in much larger RMS departures (>35%) from observations. Table 2 gives the standard deviation and correlation with observations for each factor for June, July, and August separately. The results are similar for each month except for AI, which has a lower correlation with EWP in August, perhaps indicating greater importance of convective (unresolved) ascent. The wetter months are characterized by stronger ascent (per trajectory), a greater proportion of ascending trajectories, and more wet days. Table 3 shows that the corresponding factors NT_w, AI and AF are significantly correlated. Because of the large covariances between them, the combined effect of NT_w, AI, and AF is also shown in Fig. 12 and accounts for almost all

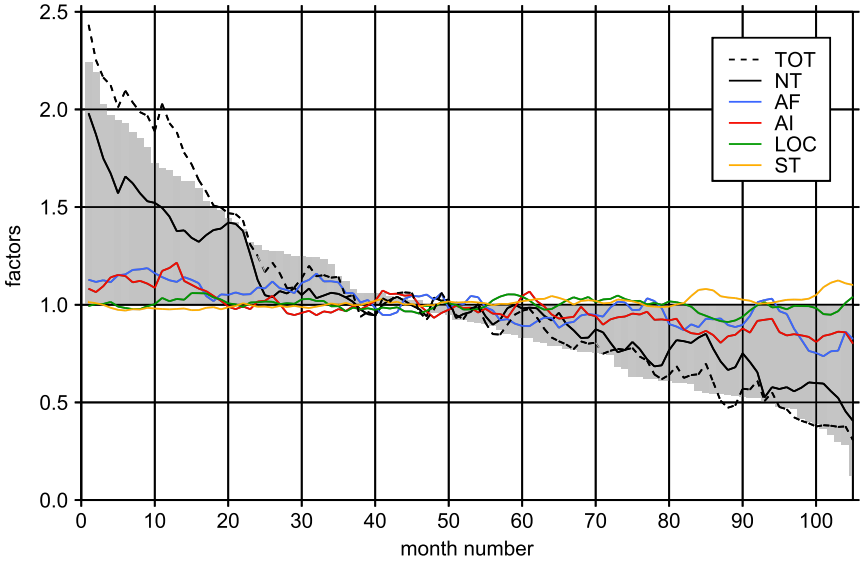

FIG. 11. As in Fig. 8, but overlaying all the individual factors influencing precipitation variability: NT (solid black, AF (blue), AI (red), LOC (green), ST (orange), and with TOT (dashed black). To reduce noise, a 5-point running average is applied to the ranked factors.

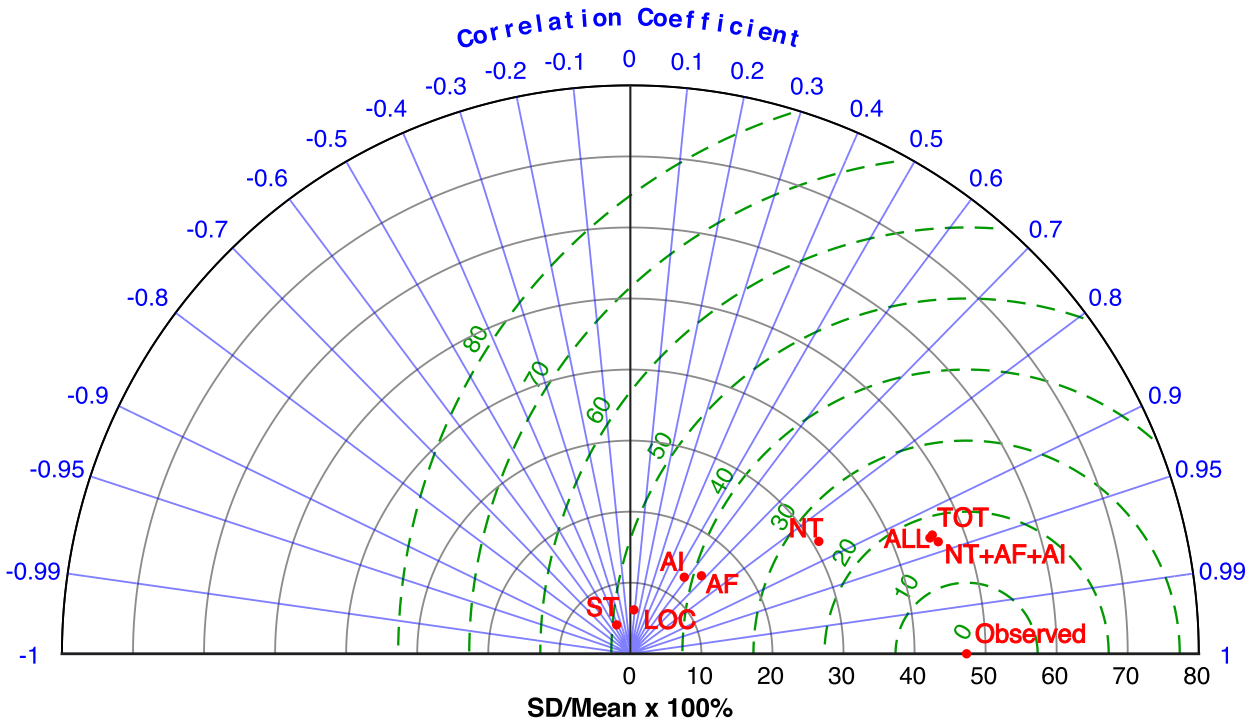

FIG. 12. Taylor diagram showing the relative skill of each of the precipitation factors compared to the observed monthly EWP time series. Each factor is located on the diagram by its normalized SD, giving the radial coordinate, and its correlation with the observations (blue numbers), giving the angle. The green lines represent the centered RMS difference (percent) between the factor and the observed time series. Each individual factor is included, as well as the combined impact of the three factors NT, AI, and AF, the total for the wet analysis type (TOT), and the combined skill of the wet and dry analyses (ALL) (red).

of the total variability in the ROTRAJ wet analyses (TOT).

In contrast, the ST factor is negatively correlated with observed monthly precipitation, revealing that surface temperature at airmass origins is anticorrelated with EWP (R between −0.34 for June and −0.51 in July, in Table 2). This is consistent with negative SST anomalies spanning the Atlantic to the west and southwest of the United Kingdom for the wet composite (Fig. 13). ST therefore acts as a weak damping factor on monthly precipitation variability (as seen in Figs. 11 and 12).

Figure 12 also shows that the skill of the LOC factor is negligible in explaining the variability (r = 0.07). Interannual variability of the shape of the origin density map is therefore unimportant for the England and Wales summer precipitation variability.

Finally, the dominant factor NT is related to cyclone count and duration. The CC and CD factors for each month in the dataset are shown in rank order of EWP in Fig. 14. The product n_{cycl} = CC × CD, representing the number of analyses with a cyclone within the vicinity of the United Kingdom, is significantly correlated with NT (R = 0.66). The implication is that precipitation variability for England and Wales is dominated by cyclone-track variability, as might be expected given its position at the end of the North Atlantic storm track.

TABLE 3. Pearson cross-correlation coefficients for all the factors in the ROTRAJ model for the wet analyses (1979–2013).

	NT	AF	AI	LOC	ST
June					
SUM	0.96	0.54	0.68	0.07	−0.29
NT	1	0.38	0.58	−0.02	−0.29
AF	—	1	0.32	0.38	−0.40
AI	—	—	1	0.22	−0.19
LOC	—	—	—	1	−0.07
July					
SUM	0.93	0.45	0.74	0.16	−0.31
NT	1	0.23	0.55	0.18	−0.29
AF	—	1	0.47	0.05	−0.42
AI	—	—	1	0.12	−0.21
LOC	—	—	—	1	−0.49
August					
SUM	0.89	0.62	0.61	0.07	−0.46
NT	1	0.42	0.33	−0.11	−0.26
AF	—	1	0.46	−0.05	−0.62
AI	—	—	1	0.12	−0.40
LOC	—	—	—	1	−0.18

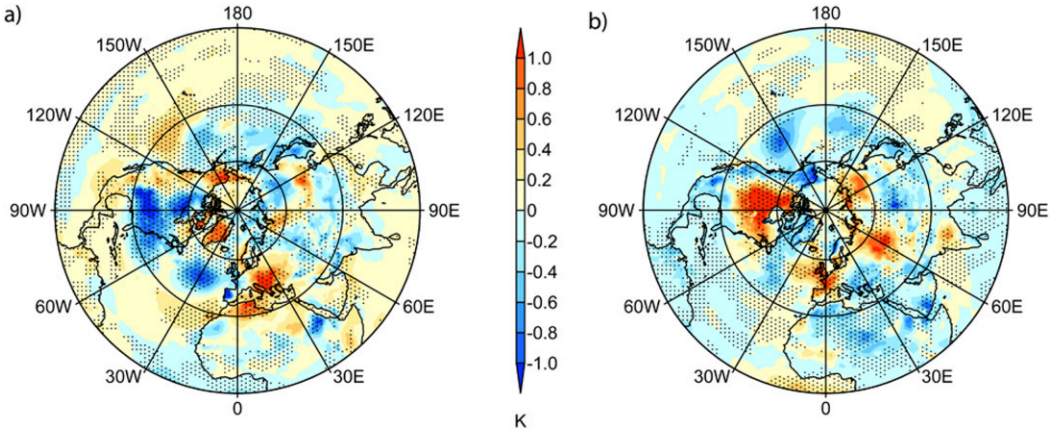

FIG. 13. The ERA-Interim JJA surface air temperature T(2 m) anomalies (K) from the climatological (1979–2013) fields for the (a) wet and (b) dry composite. Stippling represents the regions exceeding 1σ deviation from the climatological mean value.

Despite noise in the ranked data, a clear relation is found between increased cyclone duration and the wettest months. For the driest summer months only, there is an indication that the dominant factor is a low CC rather than shorter cyclone duration. This generalizes the result of the case study of summer of 2007 (Blackburn et al. 2008), which showed that the extreme precipitation over England and Wales was related to stalling of cyclones giving persistent rainfall over the region. In that case, it was a stationary Rossby wave pattern on the jet stream, with a persistent trough over the British Isles, that coupled with cyclones developing at low levels and enabled them to slow while growing through mutual interaction. De Leeuw et al. (2016) correlated EWP observations with seasonal average 500-hPa geopotential height for 1961–2013, revealing a very strong upper-level trough over the east Atlantic and the United Kingdom and also pronounced troughs over eastern North America and to the west of North America in wetter summers. Therefore, the pattern seen for summer 2007 (Blackburn et al. 2008) is representative of the other wettest months in the record. The Rossby wave pattern has a similar wavelength and phase to the leading pattern of Northern Hemisphere variability in July identified by Ding and

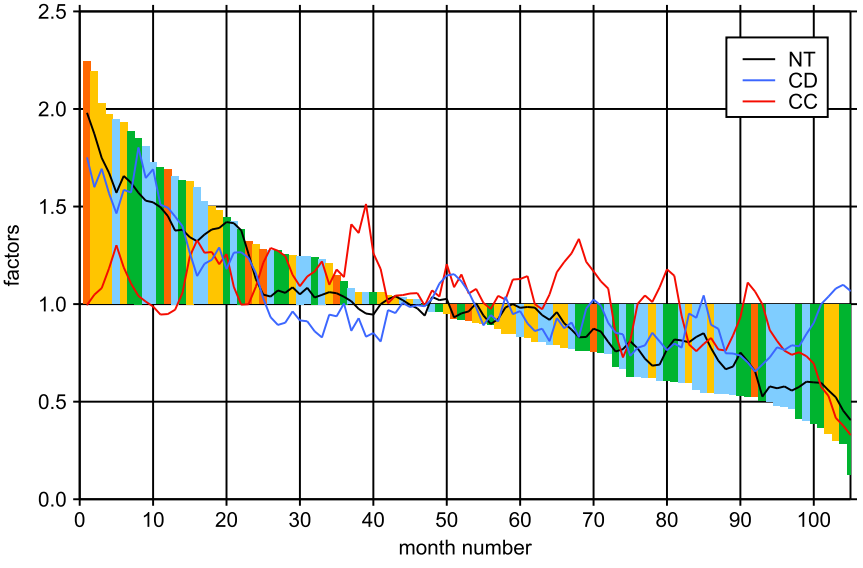

FIG. 14. The ranked monthly EWP observations for JJA 1979–2013 (bars) as in Fig. 8 and the corresponding factors for the number of wet analyses NT (black), cyclone duration CD (blue), and cyclone count CC (red).

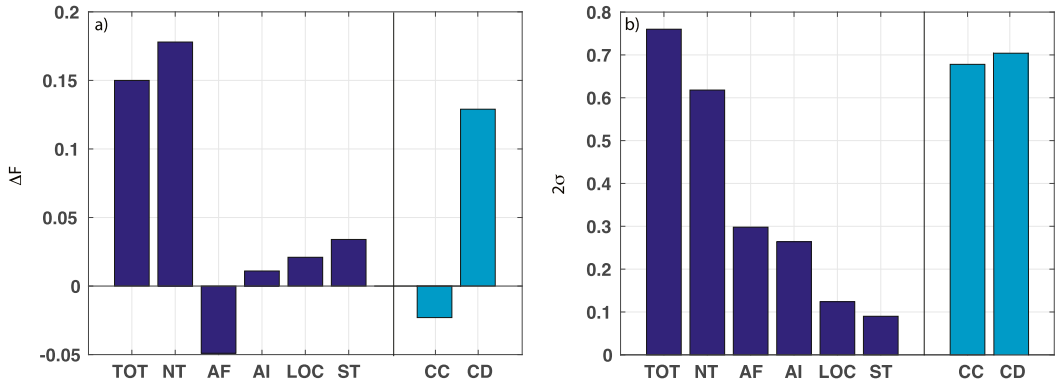

FIG. 15. (a) Seasonal average difference between the warm phase (1996–2013) and cold phase (1979–93) of the AMO for each factor, their combination (TOT), and the cyclone factors CC and CD. Positive values indicate increased precipitation during the AMO warm phase. (b) Interannual variability (represented by 2σ) for all factors. Values for each calendar month are shown in Table 2. All values are for wet analyses only, expressed as a fraction of JJA climatological average precipitation.

Wang (2005) by applying EOF analysis to the 500-hPa geopotential height.

b. *Multidecadal variability*

Sutton and Dong (2012) found that a change in summer precipitation in northern Europe in the 1990s coincided with a change in the phase of the Atlantic multidecadal oscillation (AMO), which characterizes variability of North Atlantic SSTs on multidecadal time scales. To investigate the mechanisms contributing to AMO-related variability of England and Wales summer precipitation, the trajectory model factors are analyzed for two periods, 1979–1993 and 1996–2013, based on those used by Sutton and Dong (2012), that are representative of cold and warm North Atlantic SST anomalies, respectively.

Differences in the five factors averaged separately over the warm and cold phases of the AMO ($\Delta F = \overline{F}_{\text{warm}} - \overline{F}_{\text{cold}}$) are shown in Fig. 15a. The combination of all factors (TOT) shows a precipitation increase of 15% in the AMO warm phase compared to the cold phase, which is slightly larger than the observed difference in the EWP observations between the two phases (12%). This is a significant fraction (20%) of the interannual variability of monthly precipitation (Fig. 15b).

The main contribution to the AMO-precipitation variability comes from the number of wet analyses NT, which increases by approximately 18% during the warm phase. This is associated predominantly with an increase in cyclone duration CD, with little difference in cyclone count CC. The remaining factors all have smaller contributions between AMO phases. The direct impact of surface temperature changes at the origin locations (ST) is weakly positive, contributing a 3%–4% increase in precipitation during the warm phase. This is only one-sixth of the NT factor, a similar ratio to their interannual variances. The dominance of cyclone factors between AMO phases is consistent with Dong et al. (2013), who suggested that the positive AMO-precipitation correlation is most likely related to multidecadal variability of the storm track.

It can be concluded from this comparison that understanding monthly precipitation variability and multidecadal precipitation variability are two distinct problems. The thermodynamic ST factor is anticorrelated with monthly precipitation, while it is positively correlated with summer precipitation on multidecadal time scales, Furthermore, the correlation between summer precipitation and AMO phase primarily results from changes in the North Atlantic storm track: the impact on the number and duration of cyclones giving precipitation over England and Wales is more than 6 times larger than the direct thermodynamic impact of SSTs on the water vapor content of air masses that ascend and precipitate over the region.

6. Conclusions and discussion

A Lagrangian framework is used to relate the precipitation falling over a target region to the history of air masses bringing the water vapor that condenses on ascent and precipitates. In this way, precipitation variability is connected to the physical processes that enable condensation and influence its magnitude. In this study, the ''origin'' of back trajectories is defined as the location where the water vapor mixing ratio of the air mass last increased (going forwards in time toward the ''arrival region'' where precipitation is recorded). Two categories of origin are identified depending primarily upon the location of last humidity increase relative to the top of the turbulent boundary layer (as diagnosed in the ECMWF model). The Lagrangian framework

enables a partition of precipitation rate, based on Eq. (6), between the influence of thermodynamics of saturated ascent [governed by the function $S(p, q_s)$] and the dynamics associated with the history of vertical motion (pressure change) along trajectories.

A technique is introduced that quantifies the proportion of monthly precipitation variability associated with five distinct physical mechanisms, expressed in terms of factors that combine multiplicatively to explain the total variability. The five mechanisms include the variability in 1) the surface temperature at origin locations of precipitating air masses, 2) shifts in origin locations, 3) ascent intensity, 4) the ascending fraction of total air mass over the target region, and 5) the number of ''wet analyses'' (>1 mm in 6 h averaged across the region). The Lagrangian methodology is then used to test the relative importance of each factor for the observed precipitation variability over England and Wales, a region with a dense network of reliable observations. Motivated by an exceptional sequence of wet summers over western Europe since 2007, the method is applied to the JJA season between 1979 and 2013.

The Lagrangian ROTRAJ model (Methven 1997) used in this study is used to calculate back trajectories from a 3D ''arrival grid'' over England and Wales throughout the ERA-Interim reanalysis period (over 80 million trajectories). The specific humidity change in the last 6 h before arrival is able to explain 82% of the observed daily precipitation variance, very similar to the result obtained from the ECMWF model forecasts used to produce ERA-Interim (de Leeuw et al. 2015). The ROTRAJ estimate and ECMWF forecast model estimates have a similar precipitation bias in that the PDF of precipitation rates is indistinguishable from a Weibull fit to the EWP observations aside from a uniform scaling factor of 0.77.

The origin number density maps differ significantly between the wet and dry months (Fig. 6), mainly because of changes in the mass of air contributing to precipitation over the target region. The variations in origin are a reflection of a change in the large-scale dynamics and the cyclone passage in the storm track. The largest contribution to the precipitation is from the marine boundary layer, while a smaller contribution is related to moisture origins locally (over England and Wales) and from the boundary layer over other landmasses (see Fig. 7).

Monthly precipitation variability in the United Kingdom is well described by the five factors as presented by Eqs. (13)–(16). The dominant factor in the precipitation variability is simply the number of wet analyses within each individual month NT_w (responsible for 80%–90% of the variance). The two factors related to local storm dynamics, namely, ascent intensity AI and mass fraction of ascending air AF, are found to be related to approximately 40%–60% of the variance. Because of significant cross correlations between these three cyclone-related factors (NT_w, AF, and AI), together they explain 93%–98% of the variance. Cyclone variability is therefore the dominating factor for observed summer precipitation variability over England and Wales.

The cyclone-tracking algorithm of Hodges (1994) enables the number of wet analyses to be partitioned using cyclone-track statistics. In the wettest summer months over England and Wales, it is the duration of cyclones that is anomalous rather than the number of individual cyclones. Blackburn et al. (2008) identified this as an important contributor to the extreme U.K. precipitation events that occurred in the summer of 2007. The results presented here show that this conclusion is more generally applicable to wet summer months over the past 35 yr. This result is also in agreement with Hand et al. (2004), who identified that 20% of all the observed twentieth-century extreme U.K. flood events were related to slow-moving frontal systems.

In contrast, the ST factor is anticorrelated with monthly EWP, showing that the direct thermodynamic influence of SST anomalies on water vapor content in precipitating air masses (via the Clausius–Clapeyron relation) reduces precipitation variability for locations at the end of the North Atlantic storm track (such as the United Kingdom). This arises because SST is below the climatological (1979–2013) average at the moisture origins in months with the largest precipitation accumulations over the target region. Furthermore, since the meridional variation in the surface temperature near the dominant origin locations is small, the impact of shifting the origin density map (the LOC factor) is very small for England and Wales precipitation. However, this does not imply that SST has no role to play in precipitation variability, because SST gradients can influence the dynamics of the storm track itself (e.g., Czaja and Frankignoul 2002; Brayshaw et al. 2008; Nakamura et al. 2012) and therefore the number, duration, and intensity of cyclones.

The decadal-average precipitation change associated with moving from the cold to warm phase of the Atlantic multidecadal oscillation (AMO) shows an overall increase of 15% in England and Wales summer precipitation. This is mainly associated with an increase in cyclone duration, which increases the number of wet days per month in the warm phase. The ST factor is positively correlated with summer precipitation for this AMO phase change because of the SST increase, in contrast to the negative correlation on the monthly time scale. However, the decadal precipitation change attributable to the ST factor is still 4 times smaller than that associated

with the change in cyclone duration, illustrating that changes in circulation dominate precipitation variability at the end of the North Atlantic storm track. The Lagrangian framework introduced here enables us to make this quantification by physical process rather than a purely statistical association. It seems reasonable to hypothesize that these conclusions apply to other regions at the downstream end of midlatitude storm tracks. Shepherd (2014) argued that the most uncertain aspects of the observed climate change to date, and in climate projections, are related to circulation change as opposed to global average temperature change. This study has shown that midlatitude precipitation is dominated by circulation variability (on both monthly and decadal time scales). Therefore, we can expect that precipitation changes in midlatitude regions are at least as uncertain as the storm-track changes. Application of the trajectory methodology developed here to other regions is needed to test the wider applicability of this conclusion.

Acknowledgments. We thank Harald Sodemann and two anonymous reviewers whose comments substantially improved previous versions of the manuscript. ECMWF provided data from the ERA-Interim reanalysis, and Matt Hawcroft provided cyclone-track data derived from the reanalysis. The lead author was funded by a Ph.D. scholarship from the Faculty of Science and the Department of Meteorology at the University of Reading and subsequently by The National Centre for Atmospheric Science (NCAS-Climate).

REFERENCES

Alexander, L. V., and P. D. Jones, 2000: Updated precipitation series for the U.K. and discussion of recent extremes. *Atmos. Sci. Lett.*, **1**, 142–150, doi:10.1006/asle.2000.0016.

——, and Coauthors, 2006: Global observed changes in daily climate extremes of temperature and precipitation. *J. Geophys. Res.*, **111**, D05109, doi:10.1029/2005JD006290.

Allan, R. P., and B. J. Soden, 2008: Atmospheric warming and the amplification of precipitation extremes. *Science*, **321**, 1481–1484, doi:10.1126/science.1160787.

Allen, M. R., and W. J. Ingram, 2002: Constraints on future changes in climate and the hydrologic cycle. *Nature*, **419**, 224–232, doi:10.1038/nature01092.

Blackburn, M., J. Methven, and N. Roberts, 2008: Large-scale context for the UK floods in summer 2007. *Weather*, **63**, 280–288, doi:10.1002/wea.322.

Bolton, D., 1980: The computation of equivalent potential temperature. *Mon. Wea. Rev.*, **108**, 1046–1053, doi:10.1175/1520-0493(1980)108<1046:TCOEPT>2.0.CO;2.

Brayshaw, D. J., B. Hoskins, and M. Blackburn, 2008: The storm-track response to idealized SST perturbations in an aquaplanet GCM. *J. Atmos. Sci.*, **65**, 2842–2860, doi:10.1175/2008JAS2657.1.

Czaja, A., and C. Frankignoul, 2002: Observed impact of Atlantic SST anomalies on the North Atlantic Oscillation. *J. Climate*, **15**, 606–623, doi:10.1175/1520-0442(2002)015<0606:OIOASA>2.0.CO;2.

Dee, D. P., and Coauthors, 2011: The ERA-Interim reanalysis: Configuration and performance of the data assimilation system. *Quart. J. Roy. Meteor. Soc.*, **137**, 553–597, doi:10.1002/qj.828.

de Leeuw, J., 2014: On the origin of summer precipitation variability in the UK. Ph.D. thesis, University of Reading, 256 pp.

——, J. Methven, and M. Blackburn, 2015: Evaluation of ERA-Interim reanalysis precipitation products using England and Wales observations. *Quart. J. Roy. Meteor. Soc.*, **141**, 798–806, doi:10.1002/qj.2395.

——, ——, and ——, 2016: Variability and trends in England and Wales precipitation. *Int. J. Climatol.*, **36**, 2823–2836, doi:10.1002/joc.4521.

Ding, Q., and B. Wang, 2005: Circumglobal teleconnection in the Northern Hemisphere summer. *J. Climate*, **18**, 3483–3505, doi:10.1175/JCLI3473.1.

Dong, B., R. T. Sutton, T. Woollings, and K. Hodges, 2013: Variability of the North Atlantic summer storm track: Mechanisms and impacts on European climate. *Environ. Res. Lett.*, **8**, 034037, doi:10.1088/1748-9326/8/3/034037.

Ebert, E. E., J. E. Janowiak, and C. Kidd, 2007: Comparison of near-real-time precipitation estimates from satellite observations and numerical models. *Bull. Amer. Meteor. Soc.*, **88**, 47–64, doi:10.1175/BAMS-88-1-47.

Edson, J., and Coauthors, 2007: The Coupled Boundary Layers and Air–Sea Transfer experiment in low winds. *Bull. Amer. Meteor. Soc.*, **88**, 341–356, doi:10.1175/BAMS-88-3-341.

Emanuel, K. A., 1994: *Atmospheric Convection.* Oxford University Press, 583 pp.

Frei, C., R. Schöll, S. Fukutome, J. Schmidli, and P. L. Vidale, 2006: Future change of precipitation extremes in Europe: Intercomparison of scenarios from regional climate models. *J. Geophys. Res.*, **111**, D06105, doi:10.1029/2005JD005965.

Gimeno, L., R. Nieto, A. Drumond, R. Castillo, and R. Trigo, 2013: Influence of the intensification of the major oceanic moisture sources on continental precipitation. *Geophys. Res. Lett.*, **40**, 1443–1450, doi:10.1002/grl.50338.

Gustafsson, M., D. Rayner, and D. Chen, 2010: Extreme rainfall events in southern Sweden: Where does the moisture come from? *Tellus*, **62A**, 605–616, doi:10.1111/j.1600-0870.2010.00456.x.

Hand, W. H., N. I. Fox, and C. G. Collier, 2004: A study of twentieth-century extreme rainfall events in the United Kingdom with implications for forecasting. *Meteor. Appl.*, **11**, 15–31, doi:10.1017/S1350482703001117.

Hawcroft, M. K., L. C. Shaffrey, K. I. Hodges, and H. F. Dacre, 2012: How much Northern Hemisphere precipitation is associated with extratropical cyclones? *Geophys. Res. Lett.*, **39**, L24809, doi:10.1029/2012GL053866.

Held, I. M., and B. J. Soden, 2006: Robust responses of the hydrological cycle to global warming. *J. Climate*, **19**, 5686–5699, doi:10.1175/JCLI3990.1.

Hodges, K. I., 1994: A general method for tracking analysis and its application to meteorological data. *Mon. Wea. Rev.*, **122**, 2573–2586, doi:10.1175/1520-0493(1994)122<2573:AGMFTA>2.0.CO;2.

——, 1996: Spherical nonparametric estimators applied to the UGAMP model integration for AMIP. *Mon. Wea. Rev.*, **124**, 2914–2932, doi:10.1175/1520-0493(1996)124<2914:SNEATT>2.0.CO;2.

——, 1999: Adaptive constraints for feature tracking. *Mon. Wea. Rev.*, **127**, 1362–1373, doi:10.1175/1520-0493(1999)127<1362:ACFFT>2.0.CO;2.

Holloway, C. E., and J. D. Neelin, 2009: Moisture vertical structure, column water vapor, and tropical deep convection. *J. Atmos. Sci.*, **66**, 1665–1683, doi:10.1175/2008JAS2806.1.

Huffman, G. J., R. F. Adler, D. T. Bolvin, and G. Gu, 2009: Improving the global precipitation record: GPCP version 2.1. *Geophys. Res. Lett.*, **36**, L17808, doi:10.1029/2009GL040000.

James, P., A. Stohl, N. Spichtinger, S. Eckhardt, and C. Forster, 2004: Climatological aspects of the extreme European rainfall of August 2002 and a trajectory method for estimating the associated evaporative source regions. *Nat. Hazards Earth Syst. Sci.*, **4**, 733–746, doi:10.5194/nhess-4-733-2004.

Kirtman, B., and Coauthors, 2013: Near-term climate change: Projections and predictability. *Climate Change 2013: The Physical Science Basis*, T. F. Stocker et al., Eds., Cambridge University Press, 953–1028.

Martius, O., and Coauthors, 2013: The role of upper-level dynamics and surface processes for the Pakistan flood of July 2010. *Quart. J. Roy. Meteor. Soc.*, **139**, 1780–1797, doi:10.1002/qj.2082.

Methven, J., 1997: Offline trajectories: Calculation and accuracy. U.K. Universities Global Atmospheric Modelling Programme Tech. Rep. 44, 18 pp.

——, and B. Hoskins, 1999: The advection of high-resolution tracers by low-resolution winds. *J. Atmos. Sci.*, **56**, 3262–3285, doi:10.1175/1520-0469(1999)056<3262:TAOHRT>2.0.CO;2.

——, M. Evans, P. Simmonds, and G. Spain, 2001: Estimating relationships between air mass origin and chemical composition. *J. Geophys. Res.*, **106**, 5005–5019, doi:10.1029/2000JD900694.

——, S. R. Arnold, F. M. O'Connor, H. Barjat, K. Dewey, J. Kent, and N. Brough, 2003: Estimating photochemically produced ozone throughout a domain using flight data and a Lagrangian model. *J. Geophys. Res.*, **108**, 4271, doi:10.1029/2002JD002955.

——, and Coauthors, 2006: Establishing Lagrangian connections between observations within air masses crossing the Atlantic during the International Consortium for Atmospheric Research on Transport and Transformation experiment. *J. Geophys. Res.*, **111**, D23S62, doi:10.1029/2006JD007540.

Nakamura, H., A. Nishina, and S. Minobe, 2012: Response of storm tracks to bimodal Kuroshio path states south of Japan. *J. Climate*, **25**, 7772–7779, doi:10.1175/JCLI-D-12-00326.1.

Nikulin, G., E. Kjellström, U. L. F. Hansson, G. Strandberg, and A. Ullerstig, 2011: Evaluation and future projections of temperature, precipitation and wind extremes over Europe in an ensemble of regional climate simulations. *Tellus*, **63A**, 41–55, doi:10.1111/j.1600-0870.2010.00466.x.

O'Gorman, P. A., and T. Schneider, 2009: Scaling of precipitation extremes over a wide range of climates simulated with an idealized GCM. *J. Climate*, **22**, 5676–5685, doi:10.1175/2009JCLI2701.1.

Pall, P., M. R. Allen, and D. A. Stone, 2007: Testing the Clausius–Clapeyron constraint on changes in extreme precipitation under CO_2 warming. *Climate Dyn.*, **28**, 351–363, doi:10.1007/s00382-006-0180-2.

Pauling, A., J. Luterbacher, C. Casty, and H. Wanner, 2006: Five hundred years of gridded high-resolution precipitation reconstructions over Europe and the connection to large-scale circulation. *Climate Dyn.*, **26**, 387–405, doi:10.1007/s00382-005-0090-8.

Peake, D., H. Dacre, J. Methven, and O. Coceal, 2014: Meteorological factors controlling low-level continental pollutant outflow across a coast. *Atmos. Chem. Phys.*, **14**, 10 853–10 890, doi:10.5194/acpd-14-10853-2014.

Prihodko, L., and S. N. Goward, 1997: Estimation of air temperature from remotely sensed surface observations. *Remote Sens. Environ.*, **60**, 335–346, doi:10.1016/S0034-4257(96)00216-7.

Pugh, T. A. M., and Coauthors, 2012: A Lagrangian model of air-mass photochemistry and mixing using a trajectory ensemble: The Cambridge Tropospheric Trajectory Model of Chemistry and Transport (CiTTyCAT) version 4.2. *Geosci. Model Dev.*, **5**, 193–221, doi:10.5194/gmd-5-193-2012.

Rajczak, J., P. Pall, and C. Schär, 2013: Projections of extreme precipitation events in regional climate simulations for Europe and the Alpine region. *J. Geophys. Res. Atmos.*, **118**, 3610–3626, doi:10.1002/jgrd.50297.

Shepherd, T. G., 2014: Atmospheric circulation as a source of uncertainty in climate change projections. *Nat. Geosci.*, **7**, 703–708, doi:10.1038/ngeo2253.

Skyllingstad, E. D., D. Vickers, L. Mahrt, and R. Samelson, 2007: Effects of mesoscale sea-surface temperature fronts on the marine atmospheric boundary layer. *Bound.-Layer Meteor.*, **123**, 219–237, doi:10.1007/s10546-006-9127-8.

Sodemann, H., and E. Zubler, 2010: Seasonal and inter-annual variability of the moisture sources for Alpine precipitation during 1995–2002. *Int. J. Climatol.*, **30**, 947–961, doi:10.1002/joc.1932.

——, C. Schwierz, and H. Wernli, 2008a: Interannual variability of Greenland winter precipitation sources: Lagrangian moisture diagnostic and North Atlantic Oscillation influence. *J. Geophys. Res.*, **113**, D03107, doi:10.1029/2007JD008503.

——, V. Masson-Delmotte, C. Schwierz, B. M. Vinther, and H. Wernli, 2008b: Interannual variability of Greenland winter precipitation sources: 2. Effects of North Atlantic Oscillation variability on stable isotopes in precipitation. *J. Geophys. Res.*, **113**, D12111, doi:10.1029/2007JD009416.

Stevens, B., A. Beljaars, S. Bordoni, C. Holloway, M. Köhler, S. Krueger, V. Savic-Jovcic, and Y. Zhang, 2007: On the structure of the lower troposphere in the summertime stratocumulus regime of the northeast Pacific. *Mon. Wea. Rev.*, **135**, 985–1005, doi:10.1175/MWR3427.1.

Stohl, A., and P. James, 2004: A Lagrangian analysis of the atmospheric branch of the global water cycle. Part I: Method description, validation, and demonstration for the August 2002 flooding in central Europe. *J. Hydrometeor.*, **5**, 656–678, doi:10.1175/1525-7541(2004)005<0656:ALAOTA>2.0.CO;2.

Sutton, R. T., and B. Dong, 2012: Atlantic Ocean influence on a shift in European climate in the 1990s. *Nat. Geosci.*, **5**, 788–792, doi:10.1038/ngeo1595.

Taylor, K. E., 2001: Summarizing multiple aspects of model performance in a single diagram. *J. Geophys. Res.*, **106**, 7183–7192, doi:10.1029/2000JD900719.

Trenberth, K. E., 2011: Changes in precipitation with climate change. *Climate Res.*, **47**, 123–138, doi:10.3354/cr00953.

——, A. Dai, R. M. Rasmussen, and D. B. Parsons, 2003: The changing character of precipitation. *Bull. Amer. Meteor. Soc.*, **84**, 1205–1218, doi:10.1175/BAMS-84-9-1205.

——, and Coauthors, 2007: Observations: Surface and atmospheric climate change. *Climate Change 2007: The Physical Science Basis*, S. Solomon et al., Eds., Cambridge University Press, 235–336.

Wigley, T. M. L., and P. D. Jones, 1987: England and Wales precipitation: A discussion of recent changes in variability and an update to 1985. *J. Climatol.*, **7**, 231–246, doi:10.1002/joc.3370070304.

——, J. M. Lough, and P. D. Jones, 1984: Spatial patterns of precipitation in England and Wales and a revised, homogeneous England and Wales precipitation series. *J. Climatol.*, **4**, 1–25, doi:10.1002/joc.3370040102.

Winschall, A., H. Sodemann, S. Pfahl, and H. Wernli, 2014: How important is intensified evaporation for Mediterranean precipitation extremes? *J. Geophys. Res. Atmos.*, **119**, 5240–5256, doi:10.1002/2013JD021175.